Controlling the time shape of terahertz pulses from two-color plasma by combining wavelength dispersion and laser chirp

Article *in* Applied Physics Letters · January 2024

DOI: 10.1063/5.0177262

Anna Martinez
University of Naples Federico II

Jonathan Houard
Université de Rouen

Ammar Hideur
Université de Rouen

Angela Vella
Université de Rouen

RESEARCH ARTICLE | JANUARY 10 2024

Controlling the time shape of terahertz pulses from two-color plasma by combining wavelength dispersion and laser chirp FREE

A. Martinez ; J. Houard ; A. Hideur ; D. Paparo ; A. Vella

Appl. Phys. Lett. 124, 021105 (2024)
https://doi.org/10.1063/5.0177262

Applied Physics Letters ARTICLE pubs.aip.org/aip/apl

Controlling the time shape of terahertz pulses from two-color plasma by combining wavelength dispersion and laser chirp

Cite as: Appl. Phys. Lett. **124**, 021105 (2024); doi: 10.1063/5.0177262
Submitted: 14 October 2023 · Accepted: 27 December 2023 ·
Published Online: 10 January 2024

View Online Export Citation CrossMark

A. Martinez,[1,2,3,4] J. Houard,[5] A. Hideur,[6] D. Paparo,[2,3,a)] and A. Vella[4]

AFFILIATIONS

[1]Scuola Superiore Meridionale, Largo San Marcellino, 80138 Napoli, Italy
[2]Dipartimento di Fisica "E. Pancini," Università "Federico II," Monte S. Angelo, via Cintia, 80126 Napoli, Italy
[3]CNR-ISASI, via Campi Flegrei 34, Pozzuoli, Italy
[4]Univ Rouen Normandie, INSA Rouen Normandie, CNRS, Normandie Univ, GPM UMR 6634, F-76000 Rouen, France
[5]University Rouen Normandie, INSA Rouen Normandie, CNRS, Normandie University, GPM UMR 6634, F-76000 Rouen, France
[6]CORIA CNRS, INSA, Université de Rouen Normandie, 76801 Saint Etienne du Rouvray, France

[a)]Author to whom correspondence should be addressed: domenico.paparo@cnr.it

ABSTRACT

Using a two-color plasma in air or gas allows for the generation of ultra-broadband and highly intense terahertz (THz) pulses. Precisely controlling the shape of THz pulses, particularly the carrier envelope phase, is crucial for a wide range of technological and scientific applications. Recent research has revealed that the phase difference between the fundamental laser wave and its second harmonic influences the shape of the emitted THz pulse. However, the combined impact of laser chirp and the air-dispersion-induced phase difference between the two colors has not been explored in detail. This study aims to fill this gap. The results show that both of these factors have a significant impact on the THz waveform and emitted pulse energy. Positive and negative chirps lead to distinct effects on the pulse shape. A positively chirped pump laser produces a THz waveform with a negative monopolar shape, while a negatively chirped pump laser results in a positive THz pulse shape. Additionally, our findings indicate that the relationship between THz pulse energy and chirp changes with variations in the specific phase difference between the first and second harmonics. These results underscore the importance of carefully tuning both parameters to achieve maximum generation efficiency for a given waveform.

The emission of terahertz (THz) radiation from laser plasma formed by focusing two-color femtosecond pulses in air or gas is a widely used technique due to its ultra-wide emission spectrum and relatively high THz pulse energy and peak power.[1,2] Efficiency scaling in such THz-generation schemes could be obtained by increasing the wavelength of the driving laser[1] or by optimizing the generation process.[2,3] One important aspect of this optimization is the control of the THz-optical conversion process through pulse chirp, which influences the properties of the generated THz fields. The study by Zhang *et al.*[3] delves into the influence of chirp on the generated THz power, revealing a non-monotonic dependence characterized by two maxima and a local minimum. The authors explain that, from a theoretical point of view, this trend arises from the group velocity walk-off in air. Another study by Mou *et al.*[4] investigates the effect of adding chirp to the fundamental frequency, highlighting how this results in a phase shift between the fundamental wave (FW) and the second harmonic wave (SHW). Furthermore, they conduct an in-depth study to explore the relationship between chirp and the polarization of the generated THz radiation. The findings of their study reveal that the polarization of THz waves generated by a positively chirped pump laser rotates clockwise, accompanied by an increasing phase difference between the waves. Conversely, it rotates counterclockwise when generated by a negatively chirped pump laser.

The objective of this study is to extend the previous research and investigate the impact of chirp on the temporal shape of the generated THz signal. In fact, none of the previous studies have delved into this aspect, which is crucial in various applications. For example, in molecular orientation control, it is essential that the applied THz electric field breaks the rotational parity, expressed as $\int E(t)\,dt = 0$, to induce the desired dipole force.[5] A similar condition is required in order to induce ferroelectric domain switching with precise control over the microscopic path from the initial to final structure.[6] Also, there are specific applications where precise control over the shape of the terahertz pulse is crucial. In some cases, the characteristics of the sample being analyzed determine the preference for a specific polarity. For instance, in applications where terahertz is employed to emit ions or electrons from a tip-shaped sample, the electric field experienced by the tip (near-field) becomes distorted based on the geometric and structural properties of the sample itself. This phenomenon is observed in THz-assisted atom probe tomography, for instance, where the emission and acceleration of material ions require a positive monopolar near-field pulse, while the emission and acceleration of electrons necessitate a negative monopolar near-field pulse.[7] Similarly, in THz-assisted scanning tunneling microscopy, the specific waveform of the terahertz signal can excite the lowest unoccupied molecular orbital (LUMO) states when the near field is positively monopolar, and the highest occupied molecular orbital (HOMO) states when negatively monopolar, and both states when it is bipolar.[8]

In our experiments, we employ an electro-optic detection system to measure how the THz waveform changes[9] by simultaneously varying the fundamental-beam chirp and the air-dispersion induced phase difference between the FW and its SHW. Our analysis will focus on studying both the variations in the THz time shape and its impact on the pulse energy curve. This investigation will contribute to a deeper understanding of how chirp and phase differences can be harnessed to control and optimize the energy of the generated THz pulses, their waveform, and the spectral content of THz signals. In the following, we will provide a thorough explanation of our theoretical model and the experimental setup. Then the results will be presented and carefully analyzed, with a focus on how they align with theoretical predictions derived from numerical simulations. We will also delve into the specifics of the simulations, discussing their details to further validate the results and provide a comprehensive understanding of our research findings.

In order to understand the impact of chirp on THz signal generation, we employ the photocurrent model as described by Nguyen *et al.*[10] According to this model, the THz field $\vec{E}_{THz}$ is proportional to the first derivative of the photocurrent $\vec{J}$ induced by free electrons,

$$\vec{E}_{THz}(\vec{x},t) = g\ \partial_t \vec{J}(\vec{x},t), \tag{1}$$

where the geometrical factor g originates from Jefimenko's theory.[11] More precisely, we study the problem in the local current approximation (LC), where the right-hand side of Eq. (1) is evaluated based on the laser field $\vec{E}_{\omega_0}$, and the spatial distribution of $\vec{J}$ is shaped by a delta function. At moderate intensities ($<10^{15}\,\mathrm{W\,cm^{-2}}$), the temporal shape of $\vec{J}$ follows a plasma fluid model, described by the following equation:

$$\frac{d\vec{J}(t)}{dt} + \nu_c \vec{J}(t) = \frac{e^2}{m_e} N_e\big(\big[\vec{E}(t)\big], t\big)\,\vec{E}(t). \tag{2}$$

Here, e and m_e represent the charge and mass of an electron, respectively, and $\nu_c \approx 3\ \mathrm{ps}^{-1}$ denotes the electron-neutral collision rate.[12] The density of free electrons, N_e, is governed by

$$\frac{dN_e(t)}{dt} = W(|\vec{E}(t)|)(N_a - N_e(t)), \tag{3}$$

where $N_a \approx 2.16 \times 10^{19}\ \mathrm{cm}^{-3}$ represents the initial gas density,[12] and $W(|E(t)|)$ denotes the ionization rate. In the approximation of the standard quasi-static tunneling model,[13] the ionization rate is

$$W(|\vec{E}(t)|) = \frac{\kappa}{|\vec{E}(t)|/E_{au}} e^{-\frac{\beta}{|\vec{E}(t)|/E_{au}}}, \tag{4}$$

where $\kappa = 4\omega_{au} r_H^{5/2}$, $\beta = 2/3 r_H^{3/2}$, $E_{au} = -m_e^2 e^5/\hbar^5$, and $\omega_{au} = m_e e^4/\hbar^3$, while $r_H = U_{ion}^N/U_{ion}^H$ is the ratio of the ionization potential of nitrogen ($U_{ion}^N = 15.6$ eV) to hydrogen ($U_{ion}^H = 13.6$ eV).

By applying these assumptions to Eqs. (1) and (2), the Fourier transform of the electric field is found to be

$$\hat{\vec{E}}_{THz}(\omega) = \frac{ge^2}{m_e(1 + i\nu_c/\omega)} \hat{N}_e(\omega) * \hat{\vec{E}}(\omega), \tag{5}$$

where $*$ denotes the convolution product and the hat symbol is the Fourier transform in time. The temporal behavior of the THz signal is the anti-Fourier transform of $\hat{E}_{THz}(\omega)$.

At this point, we just have to fix the mathematical expression that describes our source with chirp. In particular, here, we will use the following expression for the FW:[14]

$$E_{\omega_0}(t) = A_{\omega_0} \frac{\sqrt{1+iC}}{\sqrt{1+C^2}} \exp\left[-(1+iC)2\ln 2 \frac{t^2}{\tau^2}\right] e^{-i\omega_0 t}, \tag{6}$$

where C is the chirp parameter and ω_0 is the carrier frequency corresponding to the carrier wavelength λ_0, with $\tau = \tau_0\sqrt{1+C^2}$ and τ_0 being the FWHM durations of the stretched and transform-limited input laser pulse, respectively. Details on the derivation of this expression may be found in the supplementary material.

In the following, we will neglect the vectorial nature of the electric field and assume that it is linearly polarized: $\vec{E}(t) \equiv E(t)$. The field of the second harmonic is calculated as

$$E_{2\omega_0}(t) = \frac{\sqrt{R}}{|E_{\omega_0}(t=0)|} E_{\omega_0}^2(t) e^{-i\phi}, \tag{7}$$

where R is the fraction of FW intensity converted into the SHW intensity, ϕ accounts for the phase difference between the two waves, introduced by propagation in air from the beta-barium borate (BBO) crystal at the plasma front. In this respect, we note that our model is local, not accounting for any phase variation during propagation along the plasma filament. Despite this approximation, we show that this model demonstrates a reasonable ability to describe our experimental observations. The initial conditions in our calculations are $E(t) = E_{\omega 0}(t) + E_{2\omega 0}(t)$, $\lambda_0 = 800$ nm, and the intensity of the main and second harmonics is $I_{\omega_0} = 10^{14}\,\mathrm{W/cm^2}$ and $I_{2\omega_0} = 0.2\, I_{\omega_0}$, respectively.

For the experiment, we use a Ti:Sa laser system (Spectra Physics) which emits near-infrared pulses with 35 fs duration at a central wavelength of 800 nm; at a repetition rate of 1 kHz and maximum energy of 3 mJ per pulse. The laser beam is divided into two parts, with the higher energy beam dedicated to terahertz generation. The higher energy beam is mechanically chopped at a frequency of 500 Hz in order to increase the signal-to-noise ratio as explained below. As shown in Fig. 1, this beam is then focused in air using a 30 cm focal lens. Before reaching the focal plane, the laser beam passes through a beta-barium borate (BBO) crystal having a thickness of 100 μm, which generates the SHW with a central wavelength of 400 nm. By

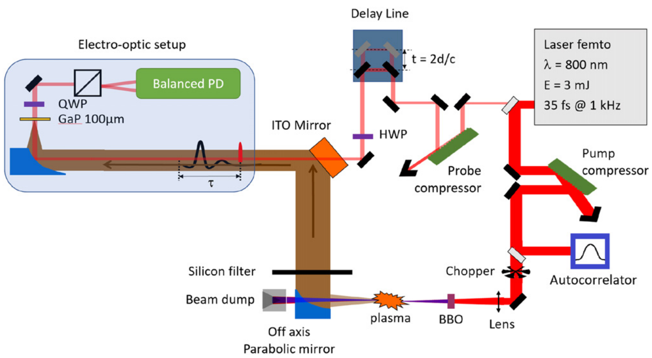

FIG. 1. Schematic diagram of the experimental setup. The pump beam passes through a BBO crystal to generate a second harmonic. Both beams are focused in air to form a plasma that produces a strong THz pulse. The probe beam is directed to the post-compression system to enable EO sampling.

combining the FW at 800 nm and its SHW, a plasma filament is generated, leading to the emission of terahertz radiation with high field strengths. The latter is directed onto the electro-optic sensing (EOS) system for further analysis. To reduce the THz absorption by air, a nitrogen environment is created from the plasma filament to the detection crystal. The probe laser beam is compressed independently from the FW beam, as shown in Fig. 1, and it is used as a probe for the EOS stage, which comprises a 100 μm thick gallium phosphide (GaP) crystal, a quarter-waveplate, and a Wollaston prism. The latter two optical elements project the probe polarization on the two circularly polarized states. These components are then detected by two balanced photodiodes connected to a lock-in amplifier (Ametek's 7265 Dual Phase) that is locked at the chopper frequency. This scheme allows a precise measurements of the polarization changes induced on the probe by the THz field impinging on the GaP crystal. By adjusting the time delay between the pump and the probe beams, a full reconstruction of the THz waveform is obtained. To manipulate the phase shift due to air dispersion, we adjusted the position of the BBO crystal relative to the plasma position. The calibration curve of the phase difference as a function of the BBO position may be found in the supplementary material. As illustrated in Fig. S1, achieving a phase variation of a fraction of π necessitates significant translations of several millimeters. Naturally, one might anticipate a potential impact on the intensity of the fundamental beam reaching the BBO crystal. However, as depicted in Fig. S1, when inducing a peak inversion by moving the BBO crystal more than 20 mm, the magnitude of the THz field remain relatively constant. This observation suggests that, given the high intensity of the fundamental wave, we could be operating in a saturation regime for second harmonic generation. This phenomenon may explain the absence of a dramatic effect upon crystal movement. Additionally, we induced chirp variation by acting on the compressor stage of the laser system. The time duration of the pump pulse measured by means of an autocorrelator (APE-pulseCheck) provides with an estimate of the chirp. As shown in Fig. 1, the latter is placed between the pump compressor and the chopper.

In Figs. 2(a)–2(c), we present the measured electro-optic traces obtained in a nitrogen environment. For each fixed BBO crystal configuration, we systematically varied the chirp, exploring both positive and negative values. By acting on the pump compressor (see Fig. 1), we can generate positively or negatively chirped pump pulses with a maximum duration of 80 fs. In the following, we indicate with a "+" and "−" exponent, a positive and negative chirp, respectively. In Fig. 2(a), the THz electric field is given for a phase shift of $\phi = \pi/2$

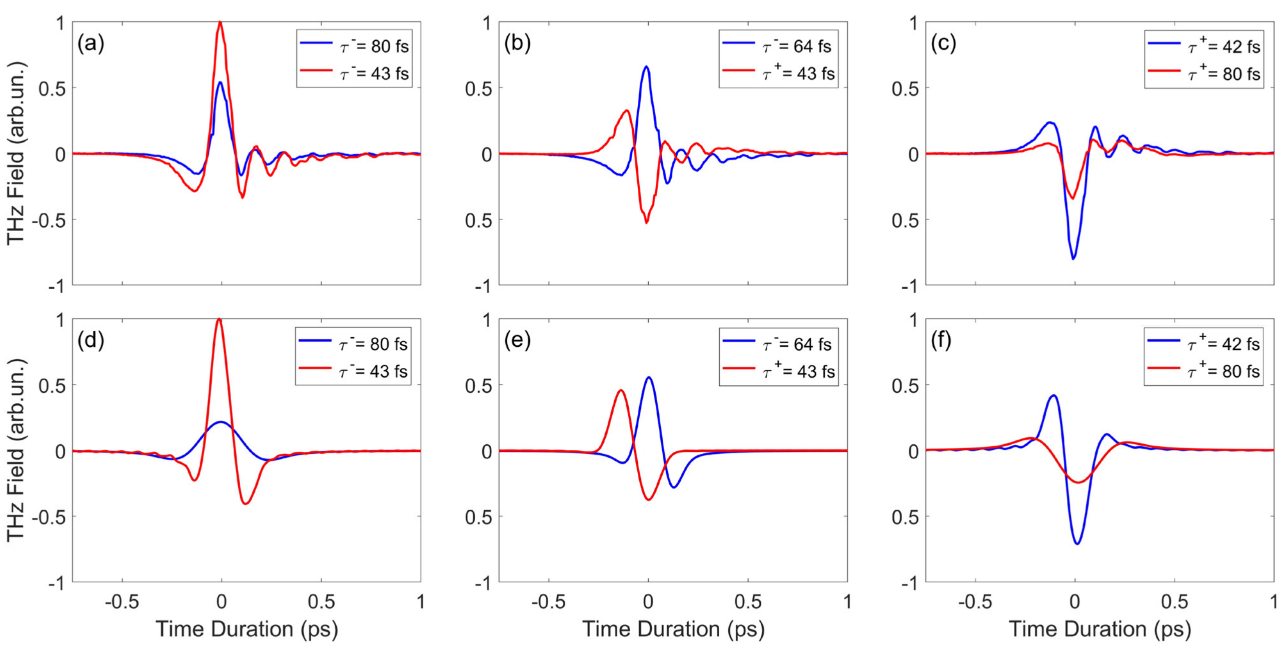

FIG. 2. In the figure, we present the measured (a)–(c) and simulated (d)–(f) traces for different positions of the BBO crystal. Specifically, in (a) and (d), the phase shift between the FHW and the SHW is $\pi/2$, in (b) and (e), it is $7\pi/9$, in (c) and (f), it is $11\pi/9$. Within each panel, the two traces correspond to different values of the chirp.

and for a FWHM duration of $\tau^- = 80$ fs and $\tau^- = 43$ fs; in (b), the phase difference is $\phi = 7\pi/9$ and $\tau^- = 64$ fs and $\tau^+ = 43$ fs; and in (c), we have $\phi = 11\pi/9$ and $\tau^+ = 42$ fs and $\tau^+ = 80$ fs. It is important to emphasize that the phase values we have reported are subject to an uncertainty of approximately $\pi/180$.

From the electro-optic traces, it is evident that a variation in chirp has a significant impact on the intensity and shape of the generated THz signal. The relationship between chirp and the variation in the shape of the THz pulse has not been documented in the scientific literature yet. Previous studies[4] have shown that a variation in chirp induces a phase difference between the first and second harmonics, which, in turn,[15] affects the shape of the THz signal. In order to study more deeply the pulse shape variations induced by chirp, we introduce the following estimator, only suitable for quasi-single-cycle pulses: $\alpha = |\max(E_{THz}(t))/\min(E_{THz}(t))|$, which contains information about the waveform of the THz electric field. In fact when $\alpha \gg 1$, the signal is positively monopolar; when $\alpha \approx 1$, the signal is bipolar; when $\alpha \ll 1$, the signal is negatively monopolar.

The analysis of α as a function of $\tau^\pm$, as shown in Fig. 3(a), provides further insights into the relationship between chirp and the shape of the THz signal. In the figures, the left side of the graphs represents results for negative chirp values, while the right side corresponds to positive chirp values. It is evident that adding negative chirp increases the positive unipolarity of the THz electric field, while adding positive chirp makes the signal more negative. It is worth noting that this trend has also been qualitatively observed through theoretical simulations based on the local photocurrent model [Fig. 3(b)]. We notice that while most of the theoretical curves closely align with the experimental results, there are some deviations, particularly evident at a phase shift of $\phi = 11\pi/9$. However, this is not unexpected, given the simplified nature of the model employed. The crucial point is that the simulations replicate the decreasing trend of α as the magnitude of $\tau^\pm$ and, hence, C increases, which further confirms the impact of chirp on the time shape of the THz signal and reinforces the validity of the experimental findings.

Commencing with the waveforms identified through the electro-optic system, we can perform a temporal integration of the square of the optical field magnitude. This process yields values, denoted as E_{THz}, which exhibits a proportionality to the optical energy within the THz pulse. Figure 4(a) illustrates these values normalized to the

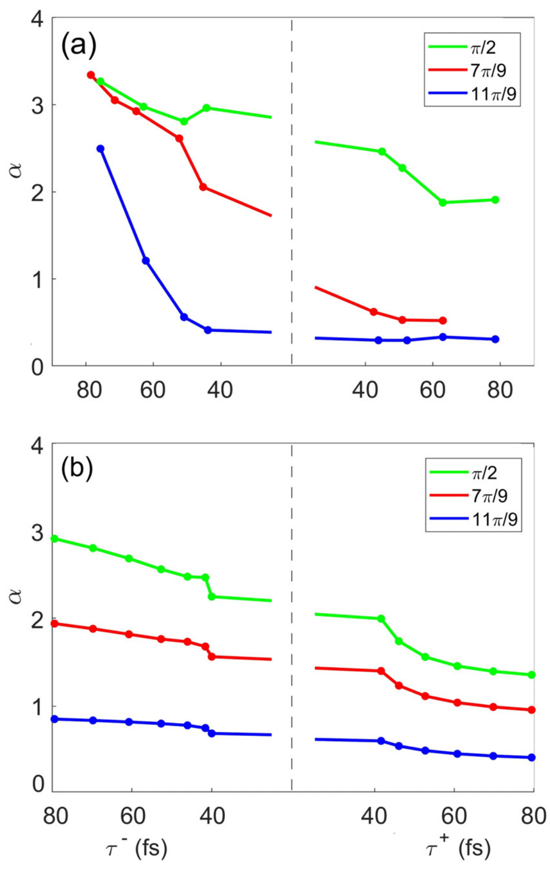

FIG. 3. Variation of α, measured via the electro-optic system (a) and simulated (b), with FWHM duration. Negative chirp values are shown on the left, and positive chirp values, on the right. The three curves correspond to measurements at different positions of the BBO crystal: green curve ($\pi/2$ phase shift), red curve ($7\pi/9$), and blue curve ($11\pi/9$).

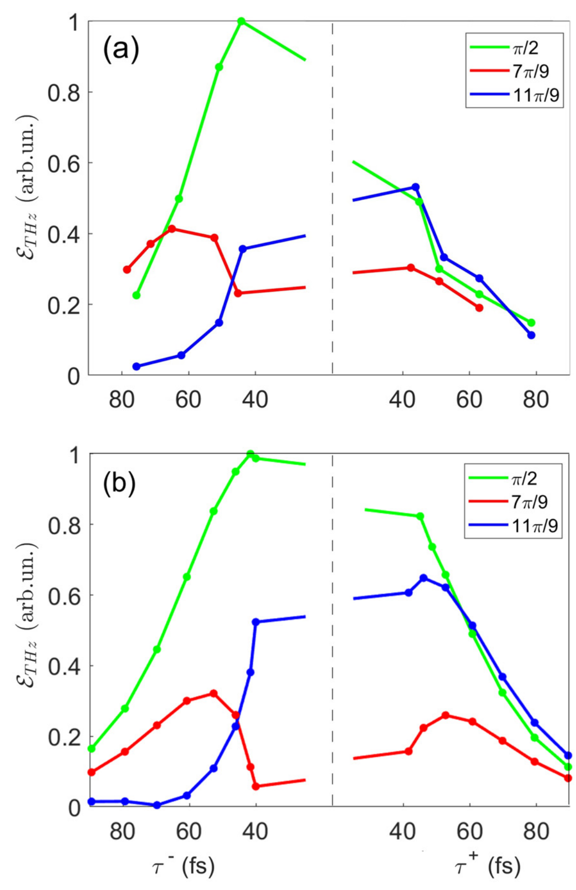

FIG. 4. Variation of THz pulse energy, measured via EOS (a) and simulated (b), with respect to $\tau^\pm$. Negative chirp values are shown on the left, and positive chirp values, on the right. The three curves correspond to measurements at different positions of the BBO crystal: green curve ($\pi/2$ phase shift), red curve ($7\pi/9$), and blue curve ($11\pi/9$).

maximum obtained energy and plotted against the phase shift angle ϕ and $\tau^{\pm}$. As before, the left side of the graph represents results for negative chirp values, while the right side corresponds to positive chirp values. The green curve corresponds to a $\pi/2$ phase shift between FW and SHW, the red curve represents a $7\pi/9$ phase shift, and the blue curve corresponds to a $11\pi/9$ phase shift. Initially, it is worth noting that the maximum pulse energy is achieved with a phase shift of $\pi/2$, which holds true for nearly all chirp values. This finding aligns with the results presented in the pioneering work by Kim *et al.*[16] Furthermore, we observe a variation in the dependence of the THz pulse energy on chirp as the specific phase difference between the first and second harmonics changes. Specifically, we find that for a $\pi/2$ phase shift between FW and SHW, the optimal THz energy generation occurs with negative chirp and a temporal duration of approximately 70 fs. Conversely, for a $11\pi/9$ phase shift, the THz pulse energy is optimized with positive chirp and a temporal duration of approximately 60 fs. Ultimately, we note that the pulse energy diminishes toward zero as the chirp increases on both sides, underscoring the impact of pulse dispersion and pulse lengthening on the FW and, consequently, SHW peak intensities.

This result is of fundamental importance as it highlights the need to adapt the chirp value based on the phase difference between FW and SHW to maximize the generated pulse energy, taking into account that a variation in chirp also modifies the shape of the signal, as discussed previously. Therefore, both parameters need to be considered to achieve the optimal conditions based on the application. In particular, when fixing the temporal duration to $\tau^{-} \approx 40$ fs and examining the temporal behavior of the pulse energy E_{THz} (see Fig. 4), we observe that for $\phi = \pi/2$, there is a higher peak compared to the one at $\phi = 11\pi/9$, which, in turn, is greater than the peak at $\phi = 7\pi/9$. We notice that, our experimental findings align closely with the photocurrent model, as illustrated in Fig. 4(b). In contrast to the results presented in Fig. 3(b), we observe a remarkable agreement between theory and experiment in this instance. This discrepancy arises from the fact that the THz pulse energy is integrated across the temporal pulse profile, whereas the parameter α is greatly influenced by the temporal fluctuations of the pulse shape.

In conclusion, our study has explored the influence of laser chirp and the air-dispersion-induced phase difference on the waveform and pulse energy of the THz signal in two-color plasma generation. Through experimental investigations and theoretical simulations, we have demonstrated that both these parameters play a crucial role in controlling various characteristics of the THz radiation. The experimental results show that the THz electric field polarity can be tailored by adjusting the chirp. By varying the latter, we were able to achieve positively monopolar, bipolar, and negatively monopolar THz signals.

Furthermore, we have explored the impact of chirp on the energy of the generated THz pulses in combination with air-dispersion-induced phase shifts between FW and SHW. Our findings indicate that the optimal chirp value for maximizing THz pulse energy depends on the specific initial phase difference, emphasizing the importance of carefully tuning both ϕ and C parameters depending on the application requirements.

The ability to control THz pulse shape and energy through phase manipulation opens up further possibilities in fields such as molecular orientation control, ferroelectric domain switching, and ion evaporation techniques, among others.

See the supplementary material for theoretical details on how air dispersion modifies a Gaussian pulse. Moreover, the calibration curve used to precisely determine the phase difference between FW and SHW as a function of the position of the BBO crystal is displayed. Additionally, the energy of the THz pulse as a function of the BBO-crystal position is also reported.

The research leading to these results has received funding from the European Union under Grant Agreement No. 101046651 "MIMOSA."

AUTHOR DECLARATIONS

Conflict of Interest

The authors have no conflicts to disclose.

Author Contributions

A. Martinez: Data curation (lead); Formal analysis (lead); Investigation (lead); Visualization (equal); Writing – original draft (equal); Writing – review & editing (equal). **J. Houard:** Conceptualization (equal); Investigation (equal); Methodology (equal); Software (lead); Supervision (equal); Validation (equal); Writing – review & editing (equal). **A. Hideur:** Conceptualization (equal); Funding acquisition (equal); Methodology (equal); Project administration (equal); Supervision (equal); Validation (equal); Writing – review & editing (equal). **D. Paparo:** Conceptualization (equal); Formal analysis (equal); Funding acquisition (equal); Project administration (equal); Supervision (equal); Validation (equal); Visualization (equal); Writing – original draft (equal); Writing – review & editing (lead). **A. Vella:** Conceptualization (equal); Data curation (equal); Formal analysis (equal); Funding acquisition (equal); Project administration (equal); Resources (equal); Supervision (equal); Validation (equal); Visualization (equal); Writing – review & editing (equal).

DATA AVAILABILITY

The data that support the findings of this study are available from the corresponding author upon reasonable request.

REFERENCES

[1] A. D. Koulouklidis, C. Gollner, V. Shumakova, V. Y. Fedorov, A. Pugžlys, A. Baltuška, and S. Tzortzakis, "Observation of extremely efficient terahertz generation from mid-infrared two-color laser filaments," Nat. Commun. **11**, 292 (2020).
[2] J. Buldt, H. Stark, M. Müller, C. Grebing, C. Jauregui, and J. Limpert, "Gas-plasma-based generation of broadband terahertz radiation with 640 mW average power," Opt. Lett. **46**, 5256–5259 (2021).
[3] Z. Zhang, N. Panov, V. A. Andreeva, and Z. Zhang, "Optimum chirp for efficient terahertz generation from two-color femtosecond pulses in air," Appl. Phys. Lett **113**, 241103 (2018).
[4] S. Mou, L. Tomarchio, A. D'Arco, M. Di Fabrizio, S. Macis, A. Curcio, L. Palumbo, S. Lupi, and M. Petrarca, "Impact of laser chirp on the polarization of terahertz from two-color plasma," Photonics Res. **11**, 978 (2023).
[5] M. Machholm and N. Henriksen, "Field-free orientation of molecules," Phys. Rev. Lett. **87**, 193001 (2001).
[6] T. Qi, Y.-H. Shin, K.-L. Yeh, K. A. Nelson, and A. M. Rappe, "Collective coherent control: Synchronization of polarization in ferroelectric $PbTiO_3$ by shaped THz fields," Phys. Rev. Lett. **102**, 247603 (2009).

[7]A. Vella, J. Houard, L. Arnoldi, M. Tang, M. Boudant, A. Ayoub, A. Normand, G. Costa, and A. Hideur, "High-resolution terahertz-driven atom probe tomography," Sci. Adv. **7**, eabd7259 (2021).
[8]S. Yoshida, Y. Arashida, H. Hirori, T. Tachizaki, A. Taninaka, H. Ueno, O. Takeuchi, and H. Shigekawa, "Terahertz scanning tunneling microscopy for visualizing ultrafast electron motion in nanoscale potential variations," ACS Photonics **8**, 315 (2021).
[9]R. Ulbricht, E. Hendry, J. Shan, T. F. Heinz, and M. Bonn, "Carrier dynamics in semiconductors studied with time-resolved terahertz spectroscopy," Rev. Mod. Phys. **83**, 543 (2011).
[10]A. Nguyen, P. G. de Alaiza Martínez, P. Thiele, S. Skupin, and L. Bergé, "THz field engineering in two-color femtosecond filaments using chirped and delayed laser pulses," New J. Phys. **20**, 033026 (2018).
[11]O. Jefimenko, *Electricity and Magnetism: An Introduction to the Theory of Electric and Magnetic Fields* (Appleton-Century-Crofts, 1966).
[12]C. D. Amico, A. Houard, S. Akturk, Y. Liu, J. L. Bloas, M. Franco, B. Prade, A. Couairon, V. T. Tikhonchuk, and A. Mysyrowicz, "Forward thz radiation emission by femtosecond filamentation in gases: Theory and experiment," New J. Phys. **10**, 013015 (2008).
[13]H. G. Roskos, M. D. Thomson, M. Kreß, and T. Löffler, "Broadband THz emission from gas plasmas induced by femtosecond optical pulses: From fundamentals to applications," Laser Photonics Rev. **1**, 349 (2007).
[14]A. Koulouklidis, V. Fedorov, and S. Tzortzakis, "Spectral bandwidth scaling laws and reconstruction of THz wave packets generated from 2-color laser plasma filaments," Phys. Rev. A **93**, 033844 (2016).
[15]R. Flender, K. Sarosi, E. Petracs, A. Borzsonyi, and V. Chikan, "Control of THz field waveform emitted from air plasma by chirping two-color laser pulses," Opt. Commun. **436**, 222 (2019).
[16]K. Y. Kim, A. J. Taylor, J. H. Glownia, and G. Rodriguez, "Coherent control of terahertz supercontinuum generation in ultrafast laser-gas interactions," Nat. Photonics **2**, 605 (2008).